Correlation Function Formalism for Triplet Excited State Decay: Combined Spin−Orbit and Nonadiabatic Couplings

Qian Peng, Yingli Niu, and Qinghua Shi

Key Laboratory of Organic Solids, Beijing National Laboratory for Molecular Sciences (BNLMS), Institute of Chemistry, Chinese Academy of Sciences, 100190 Beijing, People's Republic of China

Xing Gao and Zhigang Shuai*

Key Laboratory of Organic OptoElectronics and Molecular Engineering, Department of Chemistry, Tsinghua University, 100084 Beijing, P. R. China

Ⓢ *Supporting Information*

ABSTRACT: Based on the second-order perturbation combining spin−orbit and nonadiabatic couplings, we derived an analytical formula for nonradiative decay rate between the triplet and singlet states by using the thermal vibration correlation function (TVCF) approach. Origin displacement, distortion, and Duschinsky rotation of the potential energy surfaces are taken into accounts within the multiple harmonic oscillator model. When coupled with first-principles calculation for the anthracene, the theoretical phosphorescence spectrum is in good agreement with the experiment. Furthermore, we found that the intersystem crossing from

the first excited singlet state (S_1) to the triplet states $S_1(Bu) \rightarrow T_2(Ag)$ is forbidden by direct spin−orbit coupling at the first-order perturbation but becomes allowed through combined spin−orbit and the nonadiabatic couplings at the second-order perturbation, and the rate is calculated to be 0.26×10^8 s^{-1}, in good agreement with the experiment. Such formalism is also applied to describe the phosphorescence quantum efficiency and the temperature dependent optical emission spectrum for fac-tris(2-phenylpyridine) iridium. We predict that the radiative decay rate is 6.36×10^5 s^{-1}, the nonradiative decay rate is 5.04×10^4 s^{-1}, and the phosphorescence quantum efficiency is found to be 92.7% from T_1 to S_0, which reproduce well the corresponding experimental measurements.
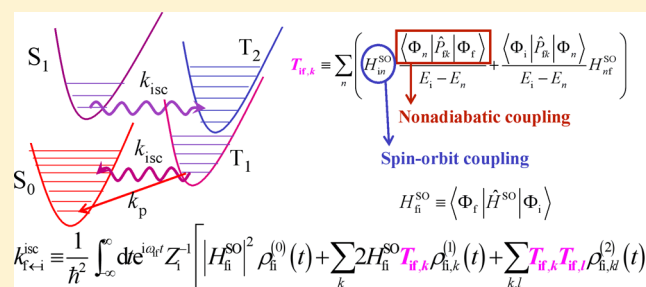
I. INTRODUCTION

White organic light-emitting diodes (WOLEDs) are considered as the promising candidates for solid state lighting application.[1−4] In WOLEDs, light emission proceeds via a recombination of injected electrons and holes to form both singlet and triplet excitons. In the conventional fluorescent emitter (singlet emitter), the triplet excitons are transferred into heat and hence are not used for the generation of light. For the phosphorescent emitter, the radiative path from the excited triplet state to the singlet ground state can be opened by the spin−orbit coupling (SOC) interaction induced by the transition metal. SOC is also able to induce an efficient transfer from the excited singlet to the light emitting triplet state. Thus, almost all the excitation energies are accumulated in the lowest excited triplet state, and inherently, the quantum efficiency may attain 100%. As a result, the WOLEDs that contain organic transition metal complexes exhibit much higher efficiency and meet the energy saving requirements. Therefore, in the WOLEDs field, a vast amount of attention has started to focus on how to design and synthesize novel highly efficient phosphorescent emitters.

Over the past decade, considerable progress in the phosphorescent emission materials has been made. In particular, a large number of iridium-based phosphors have been developed and applied in WOLEDs.[4,5] So far, the emission colors of the phosphorescent emitters can be systematically controlled and tuned from the near-UV to the near-infrared spectral range by modifying the organic ligands. However, compared to green emission molecules, the compounds that show red or blue emissions always exhibit relatively lower emission efficiencies.[6] Luminescence from molecular materials is dictated by the excited-state dynamics, namely, by the competition between radiative and the nonradiative decay processes. Molecules for WOLED application are usually quite large with >50 atoms, and the phosphorescent radiative decay time is typically around microseconds. It is impossible to run any nonadiabatic quantum dynamic simulation for the nonradiative decay process for a time scale comparable with the radiative decay time (∼micro-

seconds to milliseconds for phosphorescence). Here, we present a statistical rate analytical formalism based on second-order perturbation theory combining both spin−orbit and nonadiabatic couplings. In fact, in some cases, direct spin−orbit coupling matrix element between the singlet and triplet states could vanish by symmetry. In this case, we have to take into account the spin−vibronic coupling through second-order perturbation or the vibronic spin−orbit coupling through the first-order perturbation.[7,8] Basically, the former means the spin−orbit and nonadiabatic vibronic interactions, which must be included since the states of the same multiplicity always exist among the intermediate states in the second-order perturbation theory; the latter is the first-order derivative of the spin−orbit coupling with respect to the normal mode coordinate, which closely resembles the conventional Herzberg−Teller term of the electrical dipole transition matrix elements.[8] Marian et al. discussed the fast intersystem crossing rate driven by the first-order vibronic spin−orbit coupling for organic compounds.[9−11] To the best of our knowledge, there is no work on intersystem crossing rate through the combined spin−orbit and the nonadiabatic couplings at second-order perturbation.

In this work, based on the second perturbation theory, we derive a general intersystem crossing rate formalism including the spin-vibronic coupling by considering origin displacements, distortions, and Duschinsky rotation within a multimode harmonic oscillator model. We employ the thermal vibration correlation function (TVCF) method, which has been successfully applied to absorption and emission spectra, radiative decay rate, and the internal conversion rate from the excited singlet state to ground state by considering the Duschinsky rotation effect and the Herzberg−Teller effect.[12−14]

We have also rationalized the exotic aggregation induced emission phenomena in the novel light-emitting materials,[15−17] and the computational results have been used in designing novel light-emitting molecules with aggregation induced emission property.[18−20]

II. THEORETICAL FORMALISM

A. Intersystem Crossing Rate Constant. *General Formalism.* Based on the time-dependent second-order perturbation theory and the Born−Oppenheimer adiabatic approximation, the thermal average rate constant from the initial electronic state i with the vibrational quantum numbers v to the final electronic state f with the vibrational quantum numbers u reads:[21]

$$k_{f \leftarrow i} = \frac{2\pi}{\hbar} \sum_{v,u} P_{iv} \left| H'_{fu,iv} + \sum_{n,w} \frac{H'_{fu,nw} H'_{nw,iv}}{E_{iv} - E_{nw}} \right|^2$$
$$\times \delta(E_{iv} - E_{fu}) \tag{1}$$

Here, P_{iv} is the Boltzmann distribution function for the initial vibronic manifold; H' denotes the interaction between two different Born−Oppenheimer states; and the delta function δ is to keep the conservation of energy.

For the radiationless transitions, the interaction Hamiltonians can be considered as

$$\hat{H}' \Psi_{iv} = \hat{H}^{BO} \Phi_i(\mathbf{r}; \mathbf{Q}) \Theta_{iv}(\mathbf{Q}) + \hat{H}^{SO} \Phi_i(\mathbf{r}; \mathbf{Q}) \Theta_{iv}(\mathbf{Q}) \tag{2}$$

where $\hat{H}^{BO}$ represents nonadiabatic coupling. By neglecting the small term $\partial^2 \Phi_i / \partial Q_{fl}^2$, the coupling matrix can be expressed as

$$\langle \Phi_f \Theta_{fu} | \hat{H}^{BO} | \Phi_i \Theta_{iv} \rangle = -\hbar^2 \sum_k \left\langle \Phi_f \Theta_{fu} | \frac{\partial \Phi_i}{\partial Q_{fk}} \frac{\partial \Theta_{iv}}{\partial Q_{fk}} \right\rangle$$
$$= \sum_k \langle \Phi_f \Theta_{fu} | (\hat{P}_{fk} \Phi_i)(\hat{P}_{fk} \Theta_{iv}) \rangle \tag{3}$$

$\hat{H}^{SO}$ denotes the spin−orbit coupling, k is the index of normal mode; r and Q are the electronic and normal mode coordinates, respectively. $\hat{P}_{fk}$ is the normal momentum of the kth normal mode in the final electronic state.

Expanding eq 1, we obtain

$$k_{f \leftarrow i} = k_{f \leftarrow i}^{(0)} + k_{f \leftarrow i}^{(1)} + k_{f \leftarrow i}^{(2)} \tag{4}$$

where

$$k_{f \leftarrow i}^{(0)} = \frac{2\pi}{\hbar} \sum_{v,u} P_{iv} |H'_{fu,iv}|^2 \delta(E_{iv} - E_{fu}) \tag{5}$$

$$k_{f \leftarrow i}^{(1)} = \frac{2\pi}{\hbar} \sum_{v,u} P_{iv} 2\text{Re} \left(H'_{fu,iv} \sum_{n,w} \frac{H'_{iv,nw} H'_{nw,fu}}{E_{iv} - E_{nw}} \right)$$
$$\times \delta(E_{iv} - E_{fu}) \tag{6}$$

$$k_{f \leftarrow i}^{(2)} = \frac{2\pi}{\hbar} \sum_{v,u} P_{iv} \left| \sum_{n,w} \frac{H'_{fu,nw} H'_{nw,iv}}{E_{iv} - E_{nw}} \right|^2 \delta(E_{iv} - E_{fu}) \tag{7}$$

For the first-order contribution $k_{f \leftarrow i}^{(0)}$, due to the spin symmetry requirement, the $\hat{H}^{BO}$ term in eq 2 does not make any contribution between singlet and triplet states. So, we have

$$k_{f \leftarrow i}^{(0)} = \frac{2\pi}{\hbar} \sum_{v,u} P_{iv} |\langle \Phi_f \Theta_{fu} | \hat{H}^{SO} | \Phi_i \Theta_{iv} \rangle|^2 \delta(E_{iv} - E_{fu}) \tag{8}$$

Applying the Condon approximation, eq 8 can be further deduced to

$$k_{f \leftarrow i}^{(0)} = \frac{2\pi}{\hbar} R_{fi}^{isc} Z_i^{-1} \sum_{v,u} e^{-\beta E_v^i} |\langle \Theta_{fu} | \Theta_{iv} \rangle|^2 \delta(E_{iv} - E_{fu}) \tag{9}$$

Here, $Z_i^{-1} = \sum_{v=\{0_1, 0_2, ..., 0_N\}}^{\infty} e^{-\beta E_v^i}$ is the partition function, and $\beta = 1/(k_B T)$. N is the number of normal modes.

$$R_{fi}^{isc} \equiv |H_{fi}^{SO}|^2 \equiv |\langle \Phi_f | \hat{H}^{SO} | \Phi_i \rangle|^2 \tag{10}$$

is the spin−orbit coupling between the initial and final electronic states. Equation 9 is the simplest and the most commonly employed intersystem crossing rate formalism.

For the second term $k_{f \leftarrow i}^{(1)}$, we must simultaneously consider the contributions from terms $\hat{H}^{BO}$ and $\hat{H}^{SO}$, and their cross product term. Substituting eqs 2 and 3 into eq 6 and using the Condon approximation, neglecting the second-order of the $H_{in}^{SO} H_{nf}^{SO}$ term, we obtain

$$H'_{fu,iv} = H_{fi}^{SO} \langle \Theta_{fu} | \Theta_{iv} \rangle \tag{11}$$

$$\sum_{n,w} \frac{H'_{iv,nw}H'_{nw,fu}}{E_{iv} - E_{nw}}$$

$$= \sum_{n,w,k} \frac{\langle\Theta_{iv}|H_{in}^{SO}|\Theta_{nw}\rangle\langle\Theta_{nw}|\langle\Phi_n|\hat{P}_{fk}\Phi_f\rangle\hat{P}_{fk}|\Theta_{fu}\rangle}{E_{iv} - E_{nw}}$$

$$+ \sum_{n,w,k} \frac{\langle\Theta_{iv}|\langle\Phi_i|\hat{P}_{fk}\Phi_n\rangle\hat{P}_{fk}|\Theta_{nw}\rangle\langle\Theta_{nw}|H_{nf}^{SO}|\Theta_{fu}\rangle}{E_{iv} - E_{nw}} \tag{12}$$

Further applying Plazcek approximation, $E_{iv} - E_{nw} \approx E_i - E_n$, eq 12 can be recast into

$$\sum_{n,w} \frac{H'_{iv,nw}H'_{nw,fu}}{E_{iv} - E_{nw}} = \sum_k T_{if,k}\langle\Theta_{iv}|\hat{P}_{fk}|\Theta_{fu}\rangle \tag{13}$$

where

$$T_{if,k} \equiv \sum_n \left(H_{in}^{SO}\frac{\langle\Phi_n|\hat{P}_{fk}|\Phi_f\rangle}{E_i - E_n} + \frac{\langle\Phi_i|\hat{P}_{fk}|\Phi_n\rangle}{E_i - E_n}H_{nf}^{SO} \right) \tag{14}$$

Merging eq 11 and eq 13, we have

$$k_{f\leftarrow i}^{(1)} = \mathrm{Re}\left[\sum_k \frac{2\pi}{\hbar}2R_{fi,k}^{isc}Z_{iv}^{-1}\sum_{v,u} e^{-\beta E_v^i}P_{fu,iv,k}^{(1)}\delta(E_{iv} - E_{fu}) \right] \tag{15}$$

Here

$$R_{fi,k}^{isc} \equiv H_{fi}^{SO}T_{if,k} \tag{16}$$

and

$$P_{fu,iv,k}^{(1)} \equiv \langle\Theta_{iv}|\hat{P}_{fk}|\Theta_{fu}\rangle\langle\Theta_{fu}|\Theta_{iv}\rangle \tag{17}$$

Similarly, the third term can be recast as the following:

$$k_{f\leftarrow i}^{(2)} = \sum_{k,l} \frac{2\pi}{\hbar}R_{fi,kl}^{isc}Z_i^{-1}\sum_{v,u} e^{-\beta E_v^i}P_{fu,iv,kl}^{(2)}\delta(E_{iv} - E_{fu}) \tag{18}$$

Here

$$R_{fi,kl}^{isc} \equiv T_{if,k}T_{fi,l} \tag{19}$$

and

$$P_{fu,iv,kl}^{(2)} = \langle\Theta_{iv}|\hat{P}_{fk}|\Theta_{fu}\rangle\langle\Theta_{fu}|\hat{P}_{fl}|\Theta_{iv}\rangle \tag{20}$$

Vibration Correlation Functions. Under the harmonic oscillator model, the vibronic manifolds consist of a collection of harmonic oscillators,

$$\Theta_{iv}(\mathbf{Q}) = \prod_k \chi_{iv_k}(Q_{ik}) \tag{21}$$

$$\Theta_{fu}(\mathbf{Q}) = \prod_l \chi_{fu_l}(Q_{fl}) \tag{22}$$

and the one-dimensional harmonic oscillator Hamiltonians are

$$\hat{H}_{il} = \frac{1}{2}(\hat{P}_{il}^2 + \omega_{il}^2\hat{Q}_{il}^2) \tag{23}$$

$$\hat{H}_{fk} = \frac{1}{2}(\hat{P}_{fk}^2 + \omega_{fk}^2\hat{Q}_{fk}^2) \tag{24}$$

The delta function can be Fourier transformed as

$$\delta(E_{if} + E_v^i - E_u^f) = \frac{1}{2\pi}\int_{-\infty}^{\infty} d\tau\, e^{iE_{if}\tau}e^{i(E_v^i - E_u^f)\tau} \tag{25}$$

where

$$\tau \equiv \frac{t}{\hbar} \tag{26}$$

Substituting eqs 21−25 into the eq 9, eq 15, and eq 18, the following vibration correlation functions can be obtained:

$$k_{f\leftarrow i}^{(0)} = \frac{1}{\hbar}R_{fi}^{isc}\int_{-\infty}^{\infty} d\tau\, e^{iE_{if}\tau}Z_i^{-1}\sum_{v,u}\langle\Theta_{iv}|e^{-i\tau E_u^f}|\Theta_{fu}\rangle$$

$$\langle\Theta_{fu}|e^{-i(-\tau - i\beta)E_v^i}|\Theta_{iv}\rangle$$

$$\equiv \frac{1}{\hbar^2}R_{fi}^{isc}\int_{-\infty}^{\infty} dt\, e^{i\omega_{if}t}Z_i^{-1}\rho_{fi}^{(0)}(t) \tag{27}$$

$$k_{f\leftarrow i}^{(1)} = \mathrm{Re}\left[\frac{1}{\hbar^2}\int_{-\infty}^{\infty} dt\, e^{i\omega_{if}t}Z_i^{-1}\sum_{v,u,k}2R_{fi,k}^{isc}\langle\Theta_{iv}|\hat{P}_{fk}\,e^{-i\tau E_u^f}|\Theta_{fu}\rangle \right.$$

$$\left. \langle\Theta_{fu}|e^{-i(-\tau - i\beta)E_v^i}|\Theta_{iv}\rangle \right]$$

$$\equiv \mathrm{Re}\left[\frac{1}{\hbar^2}\int_{-\infty}^{\infty} dt\, e^{i\omega_{if}t}Z_i^{-1}\sum_k 2R_{fi,k}^{isc}\rho_{fi,k}^{(1)}(t) \right] \tag{28}$$

$$k_{f\leftarrow i}^{(2)} = \frac{1}{\hbar^2}\int_{-\infty}^{\infty} dt\, e^{i\omega_{if}t}Z_i^{-1}\sum_{v,u,k,l}R_{fi,kl}^{isc}\langle\Theta_{iv}|\hat{P}_{fk}\,e^{-i\tau E_u^f}|\Theta_{fu}\rangle$$

$$\langle\Theta_{fu}|\hat{P}_{fl}\,e^{-i(-\tau - i\beta)E_v^i}|\Theta_{iv}\rangle$$

$$\equiv \frac{1}{\hbar^2}\int_{-\infty}^{\infty} dt\, e^{i\omega_{if}t}Z_i^{-1}\sum_{k,l}R_{fi,kl}^{isc}\rho_{fi,kl}^{(2)}(t) \tag{29}$$

where

$$\omega_{if} \equiv \frac{E_{if}}{\hbar} \tag{30}$$

In eqs 27−29, the thermal vibration correlation functions are defined as

$$\rho_{fi}^{(0)}(t) \equiv \mathrm{Tr}[e^{-i\tau_f\hat{H}^f}e^{-i\tau_i\hat{H}^i}]$$

$$= \sum_{v,u}\langle\Theta_{iv}|e^{-i\tau E_u^f}|\Theta_{fu}\rangle\langle\Theta_{fu}|e^{-i(-\tau - i\beta)E_v^i}|\Theta_{iv}\rangle \tag{31}$$

$$\rho_{fi,k}^{(1)}(t) \equiv \mathrm{Tr}[\hat{P}_{fk}\,e^{-i\tau_f\hat{H}^f}e^{-i\tau_i\hat{H}^i}]$$

$$= \sum_{v,u}\langle\Theta_{iv}|\hat{P}_{fk}\,e^{-i\tau E_u^f}|\Theta_{fu}\rangle\langle\Theta_{fu}|e^{-i(-\tau - i\beta)E_v^i}|\Theta_{iv}\rangle \tag{32}$$

$$\rho_{fi,kl}^{(2)}(t) \equiv \mathrm{Tr}[\hat{P}_{fk}\,e^{-i\tau_f\hat{H}^f}\hat{P}_{fl}\,e^{-i\tau_i\hat{H}^i}]$$

$$= \sum_{v,u}R_{fi,kl}^{isc}\langle\Theta_{iv}|\hat{P}_{fk}\,e^{-i\tau E_u^f}|\Theta_{fu}\rangle\langle\Theta_{fu}|\hat{P}_{fl}\,e^{-i(-\tau - i\beta)E_v^i}|\Theta_{iv}\rangle \tag{33}$$

where

$$\tau_f \equiv \tau \tag{34}$$

$$\tau_i \equiv -\tau - i\beta \tag{35}$$

Analytical Solutions. The solutions of the $\rho_{fi}^{(0)}(t)$ and $\rho_{fi,kl}^{(2)}(t)$ have been given in ref 14 and ref 13, so here we only introduce the solution procedure for the $\rho_{fi,k}^{(1)}(t)$.

First, under the coordinate representation, by continuously inserting complete set, the vibration correlation function becomes

$$
\begin{aligned}
\rho_{\mathrm{fi},k}^{(1)}(t) &= \int \mathrm{d}\underline{x} \langle \underline{x}|\hat{P}_{fk}\, \mathrm{e}^{-i\tau_f \hat{H}^f}\, \mathrm{e}^{-i\tau_i \hat{H}^i}|\underline{x}\rangle \\
&= \int \mathrm{d}\underline{x}\mathrm{d}\underline{y}\mathrm{d}\underline{z}\mathrm{d}\underline{m}'\mathrm{d}\underline{n}' \langle \underline{x}|\hat{P}_{fk}|\underline{y}\rangle \langle \underline{y}|\mathrm{e}^{-i\tau_f \hat{H}^f}|\underline{z}\rangle \langle \underline{z}|\underline{m}'\rangle \\
&\quad \langle \underline{m}'|\mathrm{e}^{-i\tau_i \hat{H}^i}|\underline{n}'\rangle \langle \underline{n}'|\underline{x}\rangle \\
&= \int \mathrm{d}\underline{x}\mathrm{d}\underline{y}\mathrm{d}\underline{z}\mathrm{d}\underline{m}'\mathrm{d}\underline{n}' - i\hbar\delta'(x_k - y_k) \\
&\quad \prod_{j(\neq k)} \delta(x_j - y_j) \sqrt{\frac{\det[\mathbf{a}_f]}{(2\pi i\hbar)^N}} \exp\Bigg\{\frac{i}{\hbar} \\
&\quad \left[\frac{1}{2}(\underline{y}^{\mathrm{T}}\mathbf{b}_f\underline{y} + \underline{z}^{\mathrm{T}}\mathbf{b}_f\underline{z}) - \underline{y}^{\mathrm{T}}\mathbf{a}_f\underline{z}\right]\Bigg\}\delta(\underline{z} - \underline{m}') \\
&\quad \sqrt{\frac{\det[\mathbf{a}_i]}{(2\pi i\hbar)^N}} \exp\Bigg\{\frac{i}{\hbar}\left[\frac{1}{2}(\underline{m}'^{\mathrm{T}}\mathbf{b}_i\underline{m}' + \underline{n}'^{\mathrm{T}}\mathbf{b}_i\underline{n})\right. \\
&\quad \left.- \underline{m}'^{\mathrm{T}}\mathbf{a}_i\underline{n}'\right]\Bigg\}\delta(\underline{n}' - \underline{x})
\end{aligned}
\tag{36}
$$

where x, y, z... denote the final state manifold coordinate and x', y', z', ..., represent the initial state manifold, and $a_{i/f,k}(\tau_{i/f}) = \omega_{i/f,k}/\sin(\hbar\omega_{i/f,k}\tau_{i/f})$, $b_{i/f,k}(\tau_{i/f}) = \omega_{i/f,k}/\tan(\hbar\omega_{i/f,k}\tau_{i/f})$. $\mathbf{a}_{i/f}$ and $\mathbf{b}_{i/f}$ are diagonal matrices with diagonal elements $a_{i/f,k}(\tau)$ and $b_{i/f,k}(\tau)$, respectively. To solve correlation function eq 36, the Duschinsky rotation relationship between initial state and final state should be used,[13,14]

$$
Q_{il} = \sum_k S_{lk}Q_{fk} + D_l
\tag{37}
$$

where S_{lk} is the matrix element of duschinsky rotation matrix $\mathbf{S}$, and D_l is the component of displacement $\underline{D}$ between the equilibrium geometries of initial and final electronic states.

Applying multidimensional Gaussian integrations and their derivatives, the final solution of the vibration correlation function is obtained,

$$
\rho_{\mathrm{fi},k}^{(1)}(t) = -\underline{H}_k^{\mathrm{T}}\mathbf{K}^{-1}\underline{F}\sqrt{\frac{\det[\mathbf{a}_f\mathbf{a}_i]}{\det[\mathbf{K}]}} \exp\Bigg\{\frac{i}{\hbar}\left[-\frac{1}{2}\underline{F}^{\mathrm{T}}K^{-1}\underline{F}\right. \\
\left. + \underline{D}^{\mathrm{T}}E\underline{D}\right]\Bigg\}
\tag{38}
$$

Here, we define $N \times N$ matrices $\mathbf{A}$, $\mathbf{B}$, and $\mathbf{E}$,

$$
\mathbf{A} \equiv \mathbf{a}_f + \mathbf{S}^{\mathrm{T}}\mathbf{a}_i\mathbf{S}
\tag{39}
$$

$$
\mathbf{B} \equiv \mathbf{b}_f + \mathbf{S}^{\mathrm{T}}\mathbf{b}_i\mathbf{S}
\tag{40}
$$

$$
\mathbf{E} \equiv \mathbf{b}_i - \mathbf{a}_i
\tag{41}
$$

Then, we define $N \times 1$ matrices $\underline{H}_{k,1}$, $\underline{H}_{k,2}$; $2N \times 1$ matrices $\underline{H}_k$, $\underline{F}$; and $2N \times 2N$ matrix $\mathbf{K}$.

$$
\underline{H}_{k,1} \equiv [\cdots\ 0\ b_{fk}\ 0\ \cdots]^{\mathrm{T}}
\tag{42}
$$

$$
\underline{H}_{k,2} \equiv [\cdots\ 0\ -a_{fk}\ 0\ \cdots]^{\mathrm{T}}
\tag{43}
$$

$$
\underline{H}_k \equiv \begin{bmatrix} \underline{H}_{k,1} \\ \underline{H}_{k,2} \end{bmatrix}
\tag{44}
$$

$$
\underline{F} \equiv \begin{bmatrix} \underline{D}^{\mathrm{T}}\mathbf{ES} \\ \underline{D}^{\mathrm{T}}\mathbf{ES} \end{bmatrix}
\tag{45}
$$

$$
\mathbf{K} \equiv \begin{bmatrix} \mathbf{B} & -\mathbf{A} \\ -\mathbf{A} & \mathbf{B} \end{bmatrix}
\tag{46}
$$

Insert eqs 39−46 into eq 36; then, the correlation function $\rho_{\mathrm{fi},k}^{(1)}(t)$ can be obtained. The correlation functions $\rho_{\mathrm{fi}}^{(0)}(t)$ and $\rho_{\mathrm{fi},kl}^{(2)}(t)$ derived in ref 13 and ref 14 are represented as

$$
\rho_{\mathrm{fi}}^{(0)}(t) = \sqrt{\frac{\det[\mathbf{a}_f\mathbf{a}_i]}{\det[\mathbf{K}]}} \exp\left\{\frac{i}{\hbar}\left[-\frac{1}{2}\underline{F}^{\mathrm{T}}K^{-1}\underline{F} + \underline{D}^{\mathrm{T}}E\underline{D}\right]\right\}
\tag{47}
$$

$$
\rho_{\mathrm{fi},kl}^{(2)}(t) = \rho_{\mathrm{fi}}^{(0)}(t)\{i\hbar\mathrm{Tr}[\mathbf{G}_{kl}\mathbf{K}^{-1}] + (\mathbf{K}^{-1}\underline{F})^{\mathrm{T}}\mathbf{G}_{kl}(\mathbf{K}^{-1}\underline{F}) \\
- \underline{H}_{kl}^{\mathrm{T}}\mathbf{K}^{-1}\underline{F}\}
\tag{48}
$$

where

$$
\underline{H}_{kl,1} \equiv [\cdots\ 0\ b_{fk}[\underline{D}^{\mathrm{T}}\mathbf{ES}]_{l\to k}\ 0\ \cdots]^{\mathrm{T}}
\tag{49}
$$

$$
\underline{H}_{kl,2} = [\cdots\ 0\ -a_{fk}[\underline{D}^{\mathrm{T}}\mathbf{ES}]_{l\to k}\ 0\ \cdots]^{\mathrm{T}}
\tag{50}
$$

$$
\underline{H}_{kl} = \begin{bmatrix} \underline{H}_{kl,1} \\ \underline{H}_{kl,2} \end{bmatrix}
\tag{51}
$$

$$
\mathbf{G}_{kl} = \begin{bmatrix} \mathbf{G}_{kl,11} & \mathbf{G}_{kl,12} \\ \mathbf{G}_{kl,21} & \mathbf{G}_{kl,22} \end{bmatrix}
\tag{52}
$$

$$
\mathbf{G}_{kl,11} = \begin{bmatrix} \cdots \\ 0 \\ -b_{fk}[\mathbf{S}^{\mathrm{T}}\mathbf{a}_i\mathbf{S}]_{l\to k} \\ 0 \\ \cdots \end{bmatrix}
\tag{53}
$$

$$
\mathbf{G}_{kl,12} = \begin{bmatrix} \cdots \\ 0 \\ b_{fk}[\mathbf{S}^{\mathrm{T}}\mathbf{b}_i\mathbf{S}]_{l\to k} \\ 0 \\ \cdots \end{bmatrix}
\tag{54}
$$

$$
\mathbf{G}_{kl,21} = \begin{bmatrix} \cdots \\ 0 \\ a_{fk}[\mathbf{S}^{\mathrm{T}}\mathbf{a}_i\mathbf{S}]_{l\to k} \\ 0 \\ \cdots \end{bmatrix}
\tag{55}
$$

$$
\mathbf{G}_{kl,22} = \begin{bmatrix} \cdots \\ 0 \\ -a_{fk}[\mathbf{S}^{\mathrm{T}}\mathbf{b}_i\mathbf{S}]_{l\to k} \\ 0 \\ \cdots \end{bmatrix}
\tag{56}
$$

$[\mathbf{S}^{\mathrm{T}}\mathbf{a}_i\mathbf{S}]_{l\to k}$ is the lth row of matrix $[\mathbf{S}^{\mathrm{T}}\mathbf{a}_i\mathbf{S}]$, which is multiplied by $-b_{fk}$ and inserted into the kth row of $\mathbf{G}_{kl,11}$. The remaining rows of $\mathbf{G}_{kl,11}$ are null. $[\underline{D}^{\mathrm{T}}\mathbf{ES}]_{l\to k}$ is the lth element of the row matrix $[\underline{D}^{\mathrm{T}}\mathbf{ES}]$, which is multiplied by b_{fk} and inserted into the kth row of $\underline{H}_{kl,1}$. The remaining elements of $\underline{H}_{kl,1}$ are null.

Nonadiabatic Electronic Coupling. Based on the first-order perturbation theory, the nonadiabatic electronic coupling can be written as

$$\left\langle \Phi_f \middle| \frac{\partial \Phi_i}{\partial Q_{fk}} \right\rangle \approx \frac{\left\langle \Phi_f^0 \middle| \frac{\partial V}{\partial Q_{fk}} \middle| \Phi_i^0 \right\rangle}{E(\Phi_i^0) - E(\Phi_f^0)} \tag{57}$$

Using the following relations,

$$L_{f\sigma j,k} = \frac{\partial q_{\sigma j}}{\partial Q_{fk}} \tag{58}$$

$$q_{\sigma j} = \sqrt{M_\sigma} R_{\sigma j} \tag{59}$$

where σ is the index of nuclei and $j = x,y,z$. $L_{f\sigma j,k}$ is the transformation matrix element of normal mode in the final electronic state. $R_{\sigma j}$ is the Cartesian coordinate of the σth atom along j direction. The coupling can be recast as

$$\left\langle \Phi_f \middle| \frac{\partial \Phi_i}{\partial Q_{fk}} \right\rangle = \sum_\sigma^{\{nuclei\}} \sum_j^{x,y,z} M_\sigma^{-1/2} \tau_{f \leftarrow i,\sigma j} L_{f\sigma j,k} \tag{60}$$

where $\tau_{f \leftarrow i,\sigma j}$ is defined as

$$\tau_{f \leftarrow i,\sigma j} \equiv \frac{\left\langle \Phi_f^0 \middle| \frac{\partial V}{\partial R_{\sigma j}} \middle| \Phi_i^0 \right\rangle}{E(\Phi_i^0) - E(\Phi_f^0)} \tag{61}$$

The nonadiabatic electronic coupling $\tau_{f \leftarrow i,\sigma j}$ can be calculated at the level of CASSCF in the MOLPRO program.[22]

B. Phosphorescence Spectrum and Radiative Decay Rate. Generally, the spontaneous emission spectrum is expressed as

$$\sigma_{em}(\omega, T) = \frac{4\omega^3}{3c^3} \sum_{v,u} P_{iv}(T) |\langle \Theta_{fu} | \mu_{fi} | \Theta_{iv} \rangle|^2$$
$$\times \delta(E_{iv} - E_{fu} - \hbar\omega) \tag{62}$$

Here, c is the velocity of light in vacuum. $\mu_{fi} = \langle \Phi_f | \hat{\mu} | \Phi_i \rangle$ is the electric transition dipole moment.

The optical transition between singlet and triplet states is forbidden. If the spin−orbit coupling is considered, the pure singlet or triplet becomes mixed state. Using the first-order perturbation theory, the mixed singlet and triplet electronic states read

$$|S'\rangle = |S\rangle + \sum_n^{\{triplets\}} \sum_{m=-1}^{1} \frac{\langle {}^3n_m | \hat{H}^{SO} | S \rangle}{{}^1E_S - {}^3E_n} | {}^3n_m \rangle \tag{63}$$

and

$$|T_m'\rangle = |T_m\rangle + \sum_k^{\{singlets\}} \frac{\langle {}^1k | \hat{H}^{SO} | T_m \rangle}{{}^3E_T - {}^1E_k} | {}^1k \rangle \tag{64}$$

respectively. Then, the electric dipole transition between the singlet and triplet electronic states becomes allowed and can be expressed as

$$\boldsymbol{\mu}_{S \leftarrow T_m} \equiv \langle S' | \hat{\mu} | T_m' \rangle$$
$$= \sum_n^{\{triplets\}} \sum_{m'=-1}^{1} \frac{\langle S | \hat{H}^{SO} | {}^3n_{m'} \rangle \langle {}^3n_m | \hat{\mu} | T_m \rangle}{{}^1E_S - {}^3E_n}$$
$$+ \sum_k^{\{singlets\}} \frac{\langle S | \hat{\mu} | {}^1k \rangle \langle {}^1k | \hat{H}^{SO} | T_m \rangle}{{}^3E_T - {}^1E_k} \tag{65}$$

Here, n, k are the intermediate triplet and singlet electronic states, respectively; m is the magnetic quantum number ($m = \{-1, 0, 1\}$). The total transition electric dipole moment is the average of three components:

$$|\mu_{S \leftarrow T}|^2 = \frac{1}{3} \sum_m |\mu_{S \leftarrow T_m}|^2 \tag{66}$$

Adapting the vibration correlation function method, the phosphorescence spectrum formulizm can be obtained from the relevant result above-mentioned,

$$\sigma_{em}(\omega, T) = \frac{2\omega^3}{3\pi\hbar c^3} |\mu_{S \leftarrow T}|^2 \int e^{-i\omega t} e^{i\omega_{S \leftarrow T} t} Z_i^{-1} \rho_{em}(t, T) \, dt \tag{67}$$

$$\rho_{em}(t, T) = \sqrt{\frac{\det[\mathbf{a}_S \mathbf{a}_T]}{\det[\mathbf{K}]}} \exp\left\{\frac{i}{\hbar}\left[-\frac{1}{2}\underline{F}^T \mathbf{K} \underline{F} + \underline{D}^T \mathbf{E} \underline{D}\right]\right\} \tag{68}$$

The spontaneous radiative decay rate is the integration of eq 67:

$$k_r = \int_0^\infty \sigma_{em}(\omega) \, d\omega \tag{69}$$

So far, combining with our previous results,[12,13] we have obtained a unified time-integration formalism for the fluorescence and phosphorescence spectra and the corresponding radiative decay rates, the internal conversion rate, and the intersystem crossing rate by using the thermal vibration correlation function method. The advantages lie in that (i) Duschinsky rotation mixing all the normal modes as well as the Herzberg−Teller effect are incorporated analytically; (ii) the expressions are mathematically compact and ready to deal with the operations between several simple matrices and determinants; (iii) the numerical calculations are highly efficient with the help of fast Fourier transformation technique. All the vibrational modes and all the vibrational quanta for each mode are automatically included. The scale of computation is only approximately N^3 (N is the number of normal modes), namely, matrix operation. While the computational costs in the brute-force sum-overstate implementation is up to $(a + 1)^N$, where a is a required cutoff of vibrational quanta.[23] Thus, the method provides a facile framework for application in large molecules. The disadvantage or difficulty is that the time integration might not be convergent when the excited state reorganization energy is too small. This happens for the rigid and planar molecules. In this case, we introduce a (small) Lorentzian or Gaussian dephasing factor (about a few cm^{-1}) to guarantee the numerical convergence. We will demonstrate the principle through two application examples, pure organic compound anthracene and an organo-metal iridium compound.

III. COMPUTATIONAL DETAIL

For anthracene, DFT is used to optimize the geometries and calculate the frequencies and normal modes for the ground

state (S_0) and the first excited triplet state (T_1), and TDDFT is applied for the first excited singlet state (S_1). The range-separated hybrid functional CAM-B3LYP and PVTZ basis set are adopted. Based on the optimized configuration of S_1 state, the high excitation energies are evaluated using TDDFT/ B3LYP, TDDFT/CAM-B3LYP, TDDFT/M06-2X, and CASSCF methods, respectively. Then, the spin−orbit coupling matrix elements and the nonadiabatic electronic coupling matrix elements are calculated at the level of CASSCF. All the DFT and TDDFT calculations are carried out in the Gaussian 09 program package[24] and CASSCF calculations are preformed in MOLPRO program package.[22]

For fac-tris(2-phenylpyridine) iridium, the geometry optimization and frequencies calculations are performed at S_0 and T_1 states at the level of DFT with CAM-B3LYP functional and PVTZ basis sets for C, N, H atoms and Lanl2DZ for iridium atom, which are also carried out in Gaussian 09. The transition dipole moments from the T_1 to S_0 are evaluated from the quadratic response function.[25] And the corresponding spin−orbit coupling matrix elements are computed by using the effective single-electron approximation[26,27] in linear response theory, which has been confirmed to be a good standoff between the accuracy and computational cost[28] and extensively applied.[29−32] These are carried out using PVTZ basis set for C, N, H atoms and Stuttgart/Dresden ECP basis set (SDD) for iridium atom in Dalton program.[33]

Finally, for all the investigated compounds, the correlation function of phosphorescent spectra and the radiative and the intersystem crossing rate constants are calculated using our home-built programs.

IV. RESULTS AND DISCUSSION

A. Phosphorescence Spectrum and Intersystem Crossing Rates of S_1−T_m for Anthracene. Anthracene has long been focus of both theoretical and experimental researches and a wealth of experimental and theoretical spectroscopic data are available to compare with. Therefore, it is chosen as the benchmark to validate the formalism developed in this work. First, the geometries of anthracene are optimized in the S_1, T_1, and S_0 states. In the optimizations, the DFT is adopted for S_0 and T_1, and the TDDFT is used for S_1. Subsequently, based on the vibration frequencies and normal modes computed at the optimized geometries, the normalized phosphorescent spectra are obtained at temperature T = 77 K by applying the thermal vibration correlation function formalism described in Section II, and depicted in Figure 1 in comparison with the available experimental data.

CAM-B3LYP functional presents an adiabatic transition energy 1.89 eV from T_1 to S_0, close to the CCSD(T) value of 2.00 eV.[34] The calculated maxima of the phosphorescence spectra at 77 K are 14307 cm^{-1} (1.77 eV), where a shift of 0.08 eV to the red when compared with experiment for which the peak is at 14926 cm^{-1} (1.85 eV).[35] A Gaussian broadening factor of 10 cm^{-1} is added to eliminate the sharp oscillation in the spectrum. From Figure 1, it is obvious that the calculated spectrum well reproduces the experimental observation. From our previous work,[13] it was noted that Herzberg−Teller effect for anthracene is negligible. In addition, the theoretical absorption and fluorescent spectra were found to be in good agreement with the experiment.[13] These indicate that DFT theory is appropriate to predict the equilibrium geometries, vibration frequencies and normal modes for the linear polycyclic aromatic hydrocarbons (PAHs) either in S_0, S_1, or
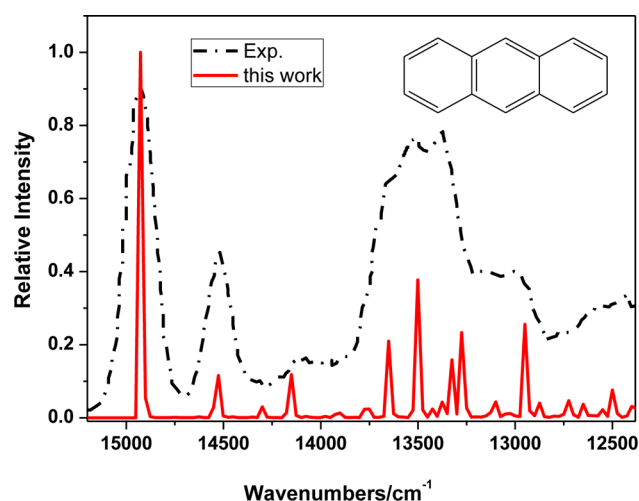

Figure 1. Calculated phosphorescent spectra with a Gaussian broadening factor 10 cm^{-1} in comparison with the experimental counterpart measured in rigid glass solution for anthracene at 77 K in ref 35.

T_1. On the other hand, our thermal vibration correlation function method works well for the PAHs.

Starting from the optimized S_1 geometry, we calculate a few low-lying excited singlet and triplet states at CASSCF and TDDFT levels (Table 1) to be used as the intermediate states

Table 1. Vertical Electronic Excitation Energies (in eV) at the Levels of CASSCF and TDDDFT Obtained at the Optimized S_1 Geometry for Anthracene (Corresponding Symmetries Are Given in Parentheses)

| states | CASSCF | TDDFT | | |
		B3LYP	CAM-B3LYP	M06-2X
S_1	4.02 (Bu)	2.79 (Bu)	3.06 (Bu)	3.09 (Bu)
S_2	4.45 (Bu)	3.70 (Bu)	3.85 (Bu)	3.88 (Bu)
S_3	4.66 (Ag)	4.14 (Ag)	4.83 (Ag)	4.87(Ag)
S_4	4.88 (Ag)	4.55 (Ag)	4.93 (Ag)	4.92 (Ag)
S_5	5.73 (Bu)	4.97 (Bu)	5.25 (Bu)	5.23 (Bu)
T_1	1.68 (Bu)	1.27 (Bu)	0.81 (Bu)	1.60 (Bu)
T_2	3.45 (Ag)	2.94 (Ag)	2.82 (Ag)	3.32 (Ag)
T_3	4.20 (Bu)	3.37 (Bu)	3.52 (Bu)	3.64 (Bu)
T_4	4.26 (Bu)	3.53 (Bu)	3.62 (Bu)	3.70 (Bu)
T_5	5.44 (Bu)	3.81 (Bu)	3.75 (Bu)	4.23 (Bu)

in eqs 6 and 7. We note that the Ag/Bu orderings of the low-lying singlet and triplet states are the same in different methods. TDDFT/B3LYP always underestimates the excitation energy as expected. The vertical excitation energy (0.81 eV) for the $T_1 \rightarrow S_0$ transition got by TDDFT/CAM-B3LYP is too low, which indicates that the TDDFT/CAM-B3LYP is not appropriate to predict the excited triplet state. Such discrepancy has already been pointed out in literature,[36,37] because the triplet excitation energy is particularly sensitive to the range-separation parameter. Nevertheless, TDDFT/M06-2X is very close to CASSCF. Therefore, TDDFT/M06-2X could be a good choose for the relatively large luminescence systems in future application. Here, since we need SOC and nonadiabatic electronic coupling elements among various excited states, which are not yet implemented in any TDDFT code, we thus stick on CASSCF calculations. We choose 9 π orbitals with 10 electrons as the active space and the state-average scheme is

considered. The SOC matrix elements are evaluated at the CASSCF level in MOLPRO program package.

From the CASSCF data (Table 1), we see that T_1 and T_2 states are below S_1, while T_3 is above.[38] So, we now look at the intersystem crossing rate of the transitions $S_1 \rightarrow T_1$ and $S_1 \rightarrow T_2$.

First, the spin−orbit coupling for singlet and triplet states and the nonadiabatic electronic coupling within the same spin-manifold are calculated at the S_1 state geometry at the CASSCF level, given in Table 2 and Figure 2, respectively. The spin−

Table 2. Calculated SOC Matrix Elements between Excited States at the Optimized S_1 Geometry using CASSCF Method

	SOC matrix elements $/i$ cm^{-1}
$\langle S_0 \| \hat{H}^{SO} \| T_{1,z} \rangle$	0.0000
$\langle S_0 \| \hat{H}^{SO} \| T_{2,z} \rangle$	0.0251
$\langle S_1 \| \hat{H}^{SO} \| T_{1,z} \rangle$	−0.0280
$\langle S_2 \| \hat{H}^{SO} \| T_{1,z} \rangle$	−0.0388
$\langle S_3 \| \hat{H}^{SO} \| T_{1,z} \rangle$	0.0000
$\langle S_4 \| \hat{H}^{SO} \| T_{1,z} \rangle$	0.0000
$\langle S_1 \| \hat{H}^{SO} \| T_{2,z} \rangle$	0.0000
$\langle S_3 \| \hat{H}^{SO} \| T_{2,z} \rangle$	0.0150
$\langle S_4 \| \hat{H}^{SO} \| T_{2,z} \rangle$	0.0000
$\langle S_1 \| \hat{H}^{SO} \| T_{3,z} \rangle$	−0.1620
$\langle S_2 \| \hat{H}^{SO} \| T_{3,z} \rangle$	0.0738
$\langle S_1 \| \hat{H}^{SO} \| T_{4,z} \rangle$	−0.0004
$\langle S_2 \| \hat{H}^{SO} \| T_{4,z} \rangle$	0.0032
$\langle S_1 \| \hat{H}^{SO} \| T_{5,z} \rangle$	0.0447
$\langle S_2 \| \hat{H}^{SO} \| T_{5,z} \rangle$	2.66×10^{-6}

orbit matrix elements are computed with Breit−Pauli spin−orbit Hamiltonian.[39,40] From Table 2, it can be seen that all the values are <1.0 cm^{-1}, which are typical for $\pi-\pi^*$ transition in planar organic molecule. Figure 2 shows the nonadiabatic electronic coupling matrix elements for different normal modes. The nonadiabatic electronic coupling matrix elements range from tens to thousands cm^{-1}.

For symmetry reasons, the direct spin−orbit coupling between S_1 (Bu) and T_2 (Ag) vanishes and the corresponding ISC is forbidden. Hence, one needs to consider the intermediate states coupled through nonadiabatic interaction to give rise indirect spin−orbit coupling, which drives the intersystem crossing from S_1 to different triplet states. Then, by checking the energy levels of the triplet and singlet states, S_2, S_3, S_4, T_1, T_3, and T_4 states are chosen as the intermediate states in eqs 28 and 29. Subsequently, based on all the electronic structure, using the thermal vibration correlation function under the second-order perturbation theory eq 4, the intersystem crossing rate of $S_1 \rightarrow T_2$ is computed. For the intersystem crossing $S_1 \rightarrow T_1$, we also consider the second-order perturbation contribution. Here, S_2, S_3, S_4, T_2, T_3, and T_4 states are chosen as the intermediate states.

We first look at the first-order term $k_{f \leftarrow i}^{(0)}$ in eq 27 for $S_1 \rightarrow T_1$ transition rate. Since anthracene is planar and rigid, the vibronic coupling is weak, presenting very small Huang−Rhys factor (Figure 3a). The integrand for the time integration is of oscillating feature. Further, the Duschinsky mode mixing effect is also very weak (Figure 3b). To guarantee the numerical convergence, we add a Gaussian factor to simulate the inhomogeneous broadening at room temperature. Here, the different broadening values 100, 50, 20, 10, and 5 cm^{-1} have been tested. The time integration interval is set to be [−10, 10] ps with an increment step of 0.001 fs. It should be noted that

the calculated rate does not depend on the broadening values. The resulting rates are 0.642×10^2 s^{-1}, 0.642×10^2 s^{-1}, 0.643×10^2 s^{-1}, 0.643×10^2 s^{-1}, and 0.643×10^2 s^{-1}, respectively, for the above chosen broadenings, which indicate that the time integration is independent of broadening factor. We present all the calculated intersystem crossing rates in Table 3. The decay rate $S_1 \rightarrow T_2$ (0.26×10^8 s^{-1}) is found to be much faster than $S_1 \rightarrow T_1$ (0.20×10^3 s^{-1}), in good agreement with the previous theoretical result[41] as well as the experimental observation in the textbook.[42] Here, it is worth mentioning that the intersystem crossing rate 0.26×10^8 s^{-1} of the $S_1 \rightarrow T_2$ is very close to that obtained from vibronically induced spin−orbit coupling.[41]

B. $T_1 \rightarrow S_0$ Transition in fac-tris(2-phenylpyridine) Iridium. Iridium-based complexes have attracted a great interest due to their applications in WOLEDs. In particular, fac-Ir(ppy)$_3$ (ppy = 2-phenyl pyridine anion) (seen in Figure 4) is the most commonly used green emitter. The photophysical properties have been extensively studied both experimentally[4,45−49] and theoretically.[30,50,51] The high resolution experimental spectra data, radiative and nonradiative transition rates at cryogenic and ambient temperatures, are available. It is our primary interest to compute both the emission spectrum at different temperature as well as the phosphorescence efficiency to compare with the experiment.

The line shape of a spectrum is a key factor to understand the photophysical properties. So, we first compare the calculated spectra with the experiment at different temperatures T = 77 K, 198 K, and 298 K, shown in Figure 5a. Usually, the emission from an electronic state takes place as purely electronic transition, for example, from a substate of T_1 to S_0 with involvement of vibrational modes. At low temperature, the transitions occur at the low-energy side of the purely electronic transition. The fine structures, caused by some active vibration modes in the radiative processes, can be well resolved. With increasing temperature, the population of three purely electronic substates of T_1 and that of molecular vibrations increase, which smear out the vibrational satellites and result in broad vibrational side bands. Experimental observation indicates that all resolved features, which stem from three different substates, disappear above about T = 25 K.[52] On the other hand, the width of an emission spectrum generally is determined by the vibronic coupling, which is induced by Franck−Condon factor, not by the electronic substates. Hence, the temperature effect is included in the Boltzmann distribution function of vibrations, and there is no additional broadening factor in the calculation.

From Figure5a, several interesting characteristics can be found for increasing temperature: (i) the vibrational satellites are smeared out, resulting in broad vibrational side bands; (ii) there is a remarkable red shift of the emission dominant peak; (iii) the intensity of emission peak reduces. The calculated maxima are 466, 506, and 509 nm at 77 K, 196 K, and 298 K, respectively, which well reproduces the experimental observations.[49] It indicates that CAM-B3LYP functional is appropriate to describe the electronic structure properties of fac-Ir(ppy)$_3$ for both S_0 and T_1. At the same time, our thermal vibration correlation function formalism is found to be suitable to describe the photophysical properties of the organo-transition metal complexes.

Huang−Rhys factor is a useful measure for the extent of geometry relaxation between two electronic states. For T_1 to S_0 transition, the calculated Huang−Rhys factors are shown in
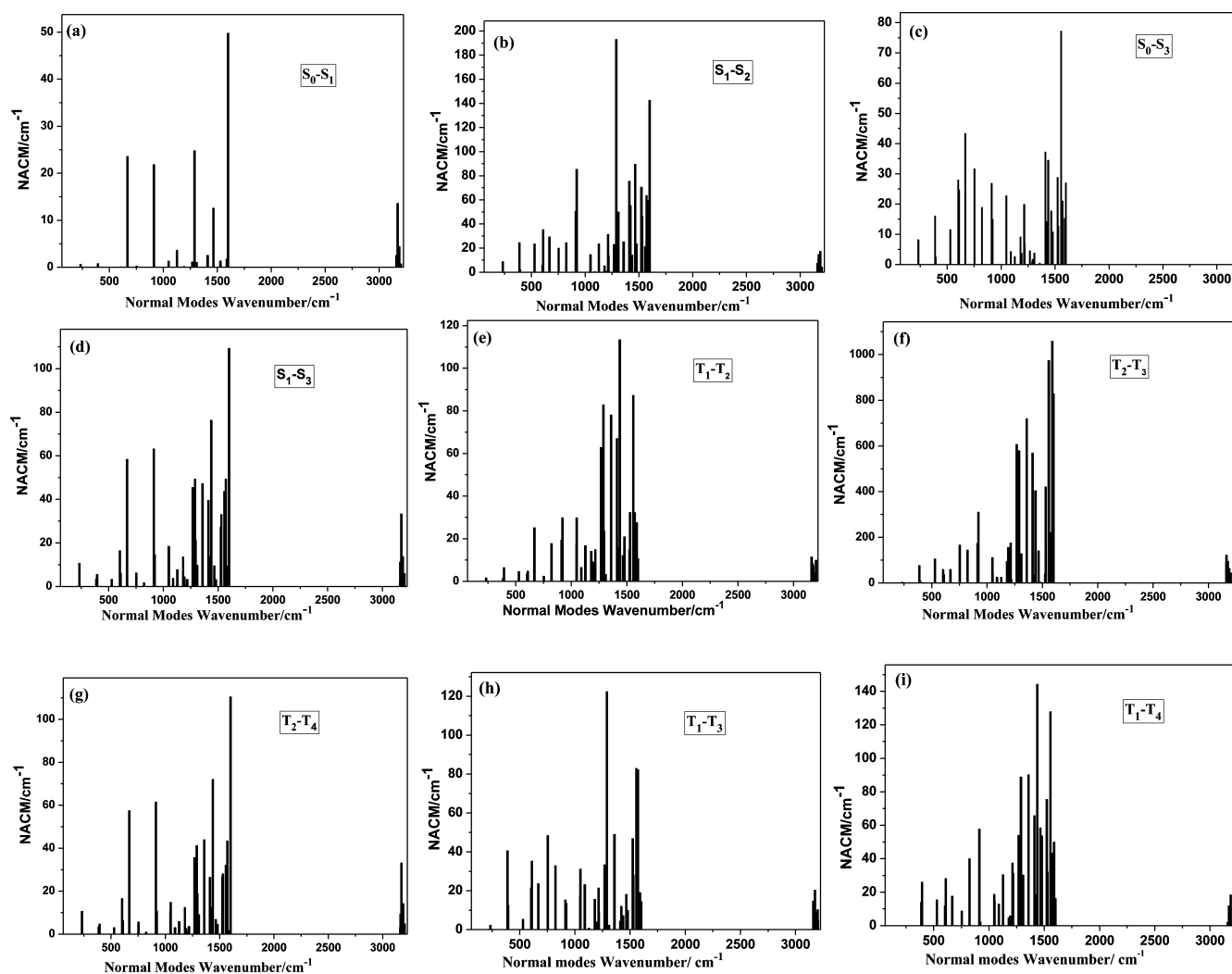
Figure 2. Selected nonadiabatic electronic coupling matrix elements between two electronic states at the optimized S_1 geometry configuration at CASSCF level.
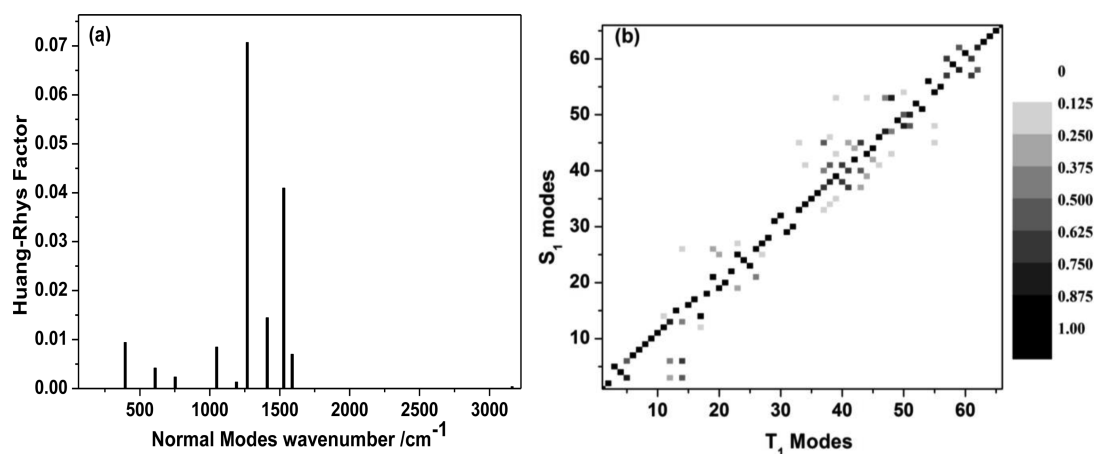

Figure 3. (a) Huang–Rhys factors in terms of S_1 surface; (b) contour map of Duschinsky rotation matrix elements (absolute value) between the S_1 and T_1 normal modes. The scale is shown at the right-hand side with interval of 0.125.

Figure 5b. The modes with large Huang–Rhys factor contribute more to the geometry relaxation.

Subsequently, we calculate the radiative and the nonradiative decay rates from T_1 to S_0 of fac-Ir$(ppy)_3$ in order to gain some insights into the light-emitting efficiency in addition to the emission spectrum. At room temperature, the spin sublevel population is equalized by spin–lattice relaxation before the excited-state decay process emission occurs. So, the excited-state decay rate constant can be simplified as average over the three substates.

1139

dx.doi.org/10.1021/ct300798t | *J. Chem. Theory Comput.* 2013, 9, 1132–1143

Table 3. Intersystem Crossing Rate (The First Term $k_{f\leftarrow i}^{(0)}$, the Second Term $k_{f\leftarrow i}^{(1)}$ and the Third Term $k_{f\leftarrow i}^{(2)}$ in eq 4) from the S_1 to the T_1 and T_2 States As Well As the Available Experimental Value (Unit: s^{-1})

	$S_1 \rightarrow T_1$	$S_1 \rightarrow T_2$	expt
$k^{(0)}$	0.64×10^2	0.00	
$k^{(1)}$	0.00	0.00	
$k^{(2)}$	0.14×10^3	0.26×10^8	
total	0.20×10^3	0.26×10^8	$0.37-0.64 \times 10^8$ [a]
			1.51×10^8 [b], $\sim 0.5 \times 10^8$ [c]

[a]Ref 43. [b]The value was measured at 293 K with the error limit $\pm 15\%$ in ref 44. [c]Ref 42.
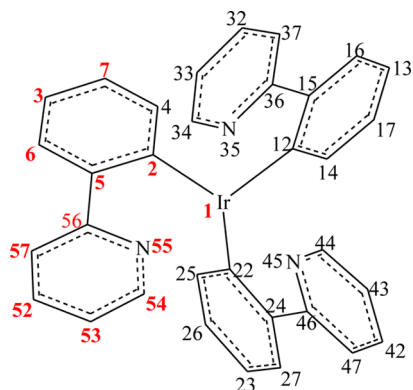

Figure 4. Molecular structure of fac-Ir(ppy)$_3$ with labeling.

The radiative rate is calculated by integrating over the emission spectrum in the whole region. The result is 6.36×10^5 s^{-1}, which is in good agreement with the experiment values of 5.6×10^5 s^{-1} obtained for Ir(ppy)$_3$ in CH$_2$Cl$_2$[52] and 6.1×10^5 s^{-1} in 2-MeTHF.[49] It is also close to the previous theoretical value 4.8×10^5 s^{-1},[53] by only considering electronic transition through Einstein spontaneous emission formula without any involvement of vibronic couplings. The spin−orbit coupling matrix element for organo-metallic compound is much larger than that in pure organic fluorescent molecules. For instance, $\langle S_0|\hat{H}^{SO}|T_1\rangle$ matrix elements are 0.66, 0.91, and 133.61 cm^{-1} for the three substates. Thus, in the perturbation theory eq 1, the first term is much larger than the second one. That is, in this case, it is reasonable to calculate the ISC rate by using the first-

order perturbation formula for fac-Ir(ppy)$_3$. The result is 5.04×10^4 s^{-1}, in line with the experimental one 3.0×10^4 s^{-1}.[52] Subsequently, the corresponding calculated phosphorescent quantum yield is 92.7%, which lies in the experimental measured range 90−96% in different solutions at room temperature. We conclude that the present computational approach can give reasonable descriptions both for the phosphorescence emission spectrum and for the quantum efficiency.

To further elucidate the structure−property relationship in organo transition metal complex Ir(ppy)$_3$, we take a look at the molecular geometry relaxation in the decay process of $T_1 \rightarrow S_0$. The main internal coordinates at S_0 and T_1, as well as the differences, are given in Table S$_1$ of the Supporting Information. It can be seen that at the S_0, the geometry symmetry is close to C_3 point group. Upon excitation to T_1, one ligand (L1) is pulled closer to the central Ir atom, corresponding to the decrease of Ir1−C2 and Ir1−N55 bond lengths, while the other ligands (L2 and L3) is pushed away, resulting in the symmetry breaking. Besides, the largest geometry relaxation occurs in L1, such as the Ir1−C2 bond, C5−C56 bond linking the phenyl and pyridine and some C−C bonds linked to C2 and N56 in L1, and so on. All the Reorganization energy characterizes the geometry relaxation. It is a sum of product of normal mode energy with the corresponding Huang−Rhys factor. Reorganization energy is a direct measure for the extent of vibronic coupling between two electronic states, which determines the width of the optical spectrum. It also indicates the nonradiative channel for the excited-state decay. Figure 6 represents normal modes contributions to the reorganization energies (detailed data seen in Supporting Information Table S2). It can be seen that the normal modes with large reorganization energies mainly appear in the high frequency region (>500 cm^{-1}). Moreover, these normal modes are mostly localized in ligand L1 rather than L2 and L3. For the sake of clarity, we depict the displacement vectors for the normal modes with the largest reorganization energies (inset of Figure 6). These normal modes mainly come from the C=C stretching vibrations in phenyl ring and pyridine ring, the deformation of phenyl ring, and the Ir−C stretching vibration.

We further decompose the organization energy into the internal coordinate relaxation given in Supporting Information
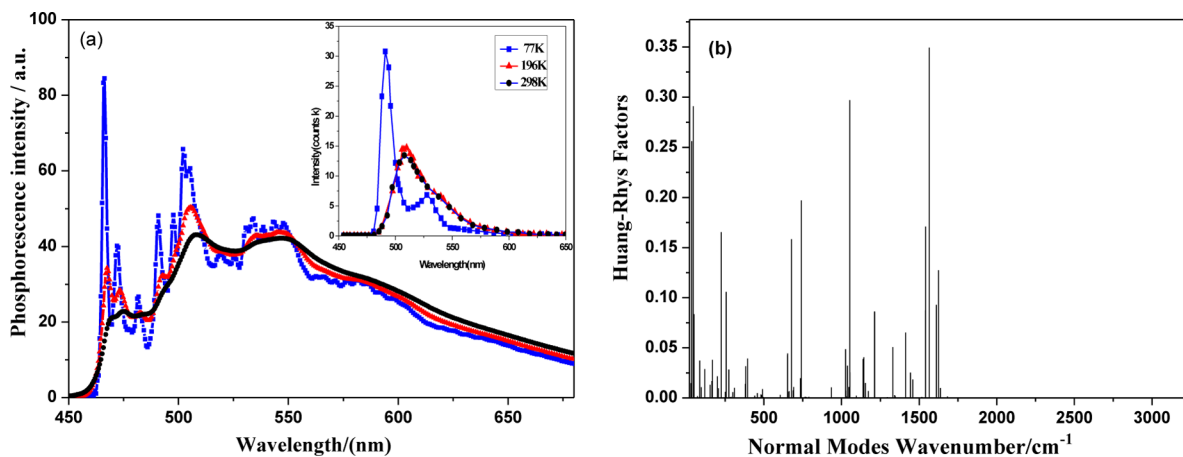

Figure 5. (a) Comparison of the calculated phosphorescent spectra with the experiment (the inset) for fac-Ir(ppy)$_3$ at 77 K, 196 K, and 298 K. (b) Calculated Huang−Rhys factors versus the normal modes between the S_0 and T_1 in term of the T_1 potential energy surface.
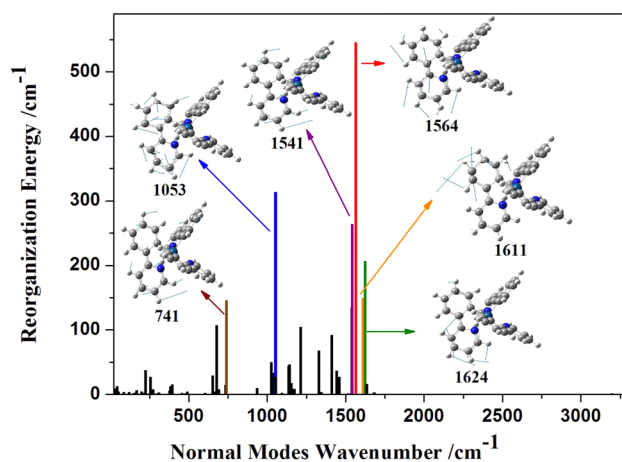
Figure 6. Calculated reorganization energies and the displacement vectors for the normal modes with the largest reorganization energies (inset).

Table S2, and the large reorganization energies and the corresponding coordinate relaxations are shown Figure 7.
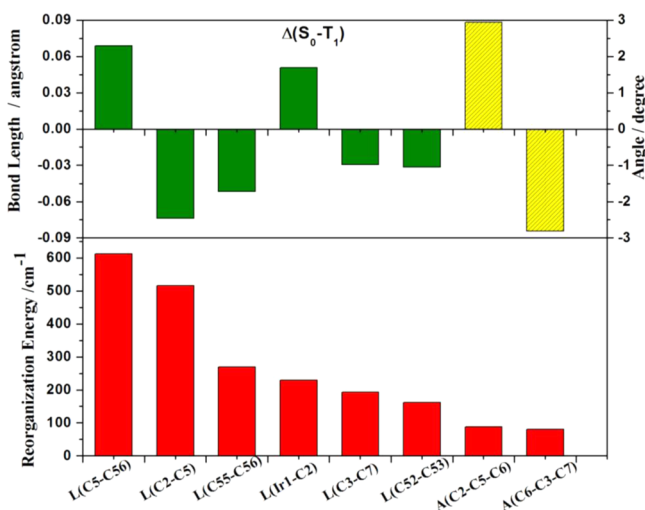

Figure 7. Large reorganization energies (bottom) and the corresponding coordinate modifications between S_0 and T_1 (top, the blank columns are for bond lengths, the column filled lines for bond angles).

Combining with the displacement vectors in Figure 6, it is seen that the largest reorganization energy (612 cm^{-1}) comes from the C5−C56 bond stretching mode (1564 cm^{-1}), whose bond length modification is -0.69 Å from T_1 to S_0. Similarly, the other structure−property relationships between coordinates, the vibration normal modes and reorganization energies are well established.

V. CONCULSION

In this study, we have presented the vibration correlation function formalisms for molecular phosphorescence spectrum, the radiative and the nonradiative decay rates arising from spin−orbit coupling of the excited states, within the harmonic oscillator model with origin displacement, distortion, and Duschinsky rotation effects. Second-order perturbation theory is applied to the intersystem crossing transition, and the spin−vibronic coupling is considered.

We first benchmark these new formalisms to examine the well-established photophysical properties of anthracene. Starting from the excited states electronic structure at the CASSCF level, the calculated phosphorescence spectrum is in good agreement with the experiment. The intersystem crossing rates from S_1 to T_1 and T_2 states are evaluated at the second-order perturbation level. It is found that $S_1{\rightarrow}T_2$ is the major decay channel with a rate constant of $0.26 \times 10^8 \text{ s}^{-1}$, while the $S_1{\rightarrow}T_1$ decay rate is only $0.20 \times 10^3 \text{ s}^{-1}$. This is in excellent agreement with the previous theoretical and experimental results. Then, we choose the most popular green OLED material Ir(ppy)_3 as an example to deepen the understanding of the decay process from the triplet to ground state in the organo-transition metal complex. By using the vibration correlation function method, we quantitatively predict the radiative decay rate to be $6.36 \times 10^5 \text{ s}^{-1}$, the nonradiative decay rate $5.04 \times 10^4 \text{ s}^{-1}$ and the resulting phosphorescence quantum efficiency is 92.7% from T_1 to S_0 for fac-Ir(ppy)_3, which well reproduce the corresponding experimental measurements. It is found that the stretching vibration motions that largely contribute to the reorganization energy mainly come from the geometry relaxations of C5−C56, C2−C5, N55−N56, and Ir1−C2 bonds. These geometry modifications not only give rise to the broadening of phosphorescence spectrum but also provide decay channels for the nonradiative intersystem crossing. These results indicate that, when coupled with the state-of-the-art quantum chemical calculations for the electronic structure, our approach can provide quantitative description for the excited state decay through the combined spin−orbit and nonadiabatic couplings.

Lastly, the present formalism is based on harmonic oscillator approximation, which becomes less accurate for 'floppy' molecules with possible anharmonicity. Indeed, for a molecular system with very few degrees of freedom, the electronic excitation energy can only be dissipated through the few channels, which requires large number of quanta of vibration, resulting in severe anharmonicity. For relatively a large system or long conjugated molecules, the electronic excitation energy becomes smaller while the number of degrees of freedom increases. As a result, the average quanta for vibration relaxation are drastically reduced, as was shown in the case of conjugated oligomers with increasing chain length.[23] Namely, such problem becomes less severe for large system, for which a nonadiabatic electron dynamics is very difficult to carry out for long time. Progress has been achieved steadily in this direction.[54]

■ APPENDIX

Analytical derivation of correlation function from eq 36 to eq 38.

Starting from eq 36, the δ functions $\delta(\underline{z} - \underline{m}')$ and $\delta(\underline{n}' - \underline{x}')$ are integrated first, giving rise to the following express:

$$\rho_{\tilde{f}i,k}^{(1)}(t) = \sqrt{\frac{\det[\mathbf{a}_f\mathbf{a}_i]}{(2\pi i\hbar)^{2N}}} \int \mathrm{d}\underline{x}\mathrm{d}\underline{y}\mathrm{d}\underline{z} - i\hbar\delta'(x_k - y_k)$$

$$\prod_{j(\neq k)}\delta(x_j - y_j) \times \exp\left\{\frac{i}{\hbar}\left[\frac{1}{2}(\underline{y}^{\mathrm{T}}\mathbf{b}_f\underline{y} + \underline{z}^{\mathrm{T}}\mathbf{b}_f\underline{z})\right.\right.$$

$$\left.- \underline{y}^{\mathrm{T}}\mathbf{a}_f\underline{z}\right\} \times \exp\left\{\frac{i}{\hbar}\left[\frac{1}{2}((\mathbf{S}\underline{z} + \underline{D})^{\mathrm{T}}\mathbf{b}_i(\mathbf{S}\underline{z} + \underline{D})\right.\right.$$

$$+ (\mathbf{S}\underline{x} + \underline{D})^{\mathrm{T}}\mathbf{b}_i(\mathbf{S}\underline{x} + \underline{D})) - (\mathbf{S}\underline{z} + \underline{D})^{\mathrm{T}}\mathbf{a}_i$$

$$\left.\left.(\mathbf{S}\underline{x} + \underline{D})\right]\right\} \tag{A1}$$

Then the δ function $\delta(x_j - y_j)$ and the first-order derivative $\delta'(x_k - y_k)$ are integrated out, leaving only 2-fold integrations,

$$\rho_{\tilde{f}i,k}^{(1)}(t) = \sqrt{\frac{\det[\mathbf{a}_f\mathbf{a}_i]}{(2\pi i\hbar)^{2N}}} \int \mathrm{d}\underline{x}\mathrm{d}\underline{z}(b_{fk}x_k - a_{fk}z_k)$$

$$\exp\left\{\frac{i}{\hbar}\left[\frac{1}{2}(\underline{x}^{\mathrm{T}}\mathbf{b}_f\underline{x} + \underline{z}^{\mathrm{T}}\mathbf{b}_f\underline{z}) - \underline{x}^{\mathrm{T}}\mathbf{a}_f\underline{z}\right]\right\}$$

$$\times \exp\left\{\frac{i}{\hbar}\left[\frac{1}{2} - \underline{x}^{\mathrm{T}}(\mathbf{S}^{\mathrm{T}}\mathbf{a}_i\mathbf{S})(\underline{x}^{\mathrm{T}}(\mathbf{S}^{\mathrm{T}}\mathbf{b}_i\mathbf{S})\underline{x}\right.\right.$$

$$\left.\left.+ \underline{z}^{\mathrm{T}}(\mathbf{S}^{\mathrm{T}}\mathbf{b}_i\mathbf{S})\underline{z})\right]\right\} \times \exp\left\{\frac{i}{\hbar}[(\underline{D}^{\mathrm{T}}(\mathbf{b}_i - \mathbf{a}_i)\mathbf{S})\right.$$

$$\left.(\underline{x} + \underline{z}) + \underline{D}^{\mathrm{T}}(\mathbf{b}_i - \mathbf{a}_i)\underline{D}]\right\} \tag{A2}$$

Appling the definitions from eq 39−41, eq A2 becomes

$$\rho_{\tilde{f}i,k}^{(1)}(t) = \sqrt{\frac{\det[\mathbf{a}_f\mathbf{a}_i]}{(2\pi i\hbar)^{2N}}} \int \mathrm{d}\underline{x}\mathrm{d}\underline{z}(b_{fk}x_k - a_{fk}z_k)$$

$$\times \exp\left\{\frac{i}{\hbar}\left[\frac{1}{2}(\underline{x}^{\mathrm{T}}\mathbf{B}\underline{x} + \underline{z}^{\mathrm{T}}\mathbf{B}\underline{z}) - \underline{x}^{\mathrm{T}}\mathbf{A}\underline{z} + (\underline{D}^{\mathrm{T}}\mathbf{ES})\right.\right.$$

$$\left.\left.(\underline{x} + \underline{z}) + \underline{D}^{\mathrm{T}}\mathbf{E}\underline{D}\right]\right\} = \sqrt{\frac{\det[\mathbf{a}_f\mathbf{a}_i]}{(2\pi i\hbar)^{2N}}}$$

$$\int \mathrm{d}\underline{x}\mathrm{d}\underline{z}\left(\left[\cdots 0 b_{fk} 0 \cdots, \cdots 0 - a_{fk} 0 \cdots\right]\begin{bmatrix}\underline{x}\\\underline{z}\end{bmatrix}\right)$$

$$\times \exp\left\{\frac{i}{\hbar}\left[\frac{1}{2}[\underline{x}^T\underline{z}^T]\begin{bmatrix}\mathbf{B} & -\mathbf{A}\\-\mathbf{A} & \mathbf{B}\end{bmatrix}\begin{bmatrix}\underline{x}\\\underline{z}\end{bmatrix} + [\underline{D}^T\mathbf{ES}, \underline{D}^T\mathbf{ES}]\right.\right.$$

$$\left.\left.\begin{bmatrix}\underline{x}\\\underline{z}\end{bmatrix} + \underline{D}^T\mathbf{E}\underline{D}\right]\right\} \tag{A3}$$

Now, we can double the dimension of the space by introducing a new multidimensional variable $\underline{y}^{\mathrm{T}} = [\underline{x}^{\mathrm{T}}, \underline{z}^{\mathrm{T}}]$ and defining new quantities in the new $2N$-dimensional space as shown in eq 42−46, the following equation is yielded

$$\rho_{\tilde{f}i,k}^{(1)}(t) = \sqrt{\frac{\det[\mathbf{a}_f\mathbf{a}_i]}{(2\pi i\hbar)^{2N}}} \int \mathrm{d}\underline{y}(\underline{H}^{\mathrm{T}}\underline{y}) \exp\left\{\frac{i}{\hbar}\left[\frac{1}{2}\underline{y}^{\mathrm{T}}\mathbf{K}\underline{y} + \underline{F}^{\mathrm{T}}\underline{y}\right.\right.$$

$$\left.\left.+ \underline{D}^{\mathrm{T}}\mathbf{E}\underline{D}\right]\right\} \tag{A4}$$

Finally, applying the multidimensional Gaussian integrations and their derivatives, the final solution eq 38 is obtained.

ASSOCIATED CONTENT

Ⓢ Supporting Information

Selected bond lengths (Å), angles and torsion angles (deg) of the S_0 and T_1 for the fac-Ir(ppy)$_3$, and their differences, the main normal modes contributions to the reorganization energy, and the decomposition of the reorganization energy onto the internal coordinate modifications are provided. This material is available free of charge via the Internet at http://pubs.acs.org/

AUTHOR INFORMATION

Corresponding Author

*E-mail: zgshuai@tsinghua.edu.cn.

Notes

The authors declare no competing financial interest.

ACKNOWLEDGMENTS

REFERENCES

(1) Kido, J.; Kimura, M.; Nagai, K. *Science* **1995**, *267*, 1332−1334.

(2) Sun, Y.; Giebink, N. C.; Kanno, H.; Ma, B.; Thompson, M. E.; Forrest, S. R. *Nature* **2006**, *440*, 908−912.

(3) Reineke, S.; Lindner, F.; Schwartz, G.; Seidler, N.; Walzer, K.; Lussem, B.; Leo, K. *Nature* **2009**, *459*, 234−238.

(4) Yersin, H.; Finkenzeller, W. J. Triplet Emitter for Organic Light-Emitting Diodes: Basic Properties. In *Highly Efficient OLEDs with Phosphorescent Materials*; Yersin, H., Ed.; Wiley-VCH Verlag GmbH & Co. KGaA: Weiheim, Germany, 2008; pp 1−98.

(5) Baldo, M. A.; O'Brien, D. F.; You, Y.; Shoustikov, A.; Sibley, S.; Thompson, M. E.; Forrest, S. R. *Nature* **1998**, *395*, 151−154.

(6) Sajoto, T.; Djurovich, P. I.; Tamayo, A.; Yousufuddin, M.; Bau, R.; Thompson, M. E.; Holmes, R. J.; Forrest, S. R. *Inorg. Chem.* **2005**, *44*, 7992−8003.

(7) Siebrand, W. Nonradiative Processes in Molecular Systems. In *Dynamics of Molecular Collisions*; Miller, W. H., Ed.; Pelnum Press: New York, 1976; pp 249−302.

(8) Lim, E. C. Vibronic Interactions and Luminescence in Aromatic Molecules with Nonbonding Electrons. In *Excited States*; Lim, E. C., Ed.; Academic Press: New York, 1977; Vol. 3, pp 305−337.

(9) Marian, C. M. *WIREs: Comput. Mol. Sci.* **2012**, *2*, 187−203.

(10) Etinski, M.; Tatchen, J.; Marian, C. M. *J. Chem. Phys.* **2011**, *134*, 154105−9.

(11) Tatchen, J.; Gilka, N.; Marian, C. M. *Phys. Chem. Chem. Phys.* **2007**, *9*, 5209−5221.

(12) Peng, Q.; Yi, Y.; Shuai, Z.; Shao, J. *J. Chem. Phys.* **2007**, *126*, 114302−8.

(13) Niu, Y.; Peng, Q.; Deng, C.; Gao, X.; Shuai, Z. *J. Phys. Chem. A* **2010**, *114*, 7817−7831.

(14) Ianconescu, R.; Pollak, E. *J. Phys. Chem. A* **2004**, *108*, 7778−7784.

(15) Peng, Q.; Yi, Y.; Shuai, Z.; Shao, J. *J. Am. Chem. Soc.* **2007**, *129*, 9333−9339.

(16) Deng, C.; Niu, Y.; Peng, Q.; Qin, A.; Shuai, Z.; Tang, B. Z. *J. Chem. Phys.* **2011**, *135*, 014304−8.

(17) Wu, Q.; Deng, C.; Peng, Q.; Niu, Y.; Shuai, Z. *J. Comput. Chem.* **2012**, *33*, 1862−1869.

(18) Tavazzi, S.; Mora, S.; Alessandrini, L.; Silvestri, L. *J. Chem. Phys.* **2011**, *134*, 034707−8.

(19) Liu, J.; Zhong, Y.; Lam, J. W. Y.; Lu, P.; Hong, Y.; Yu, Y.; Yue, Y.; Faisal, M.; Sung, H. H. Y.; Williams, I. D.; Wong, K. S.; Tang, B. Z. *Macromolecules* **2010**, *43*, 4921−4936.

(20) Hong, Y.; Lam, J. W. Y.; Tang, B. Z. *Chem. Soc. Rev.* **2011**, *40*, 5361−5388.

(21) Lin, S. H.; Chang, C. H.; Liang, K. K.; Chang, R.; Shiu, Y. J.; Zhang, J. M.; Yang, T. S.; Hayashi, M.; Hsu, F. C. *Advances in Chemical Physics*. John Wiley & Sons: New York, 2002; Vol *121*, pp 1−88.

(22) Werner, H. J.; Knowles, P. J.; Lindh, R.; Manby, F. R.; Schutz, M.; Others, A. *MOLPRO*, version 2009.1, a package of ab initio programs; University College Cardiff Consultants Limited: Cardiff, 2009; available online: http://www.molpro.net.

(23) Jiang, Y.; Peng, Q.; Gao, X.; Shuai, Z.; Niu, Y.; Lin, S. H. *J. Mater. Chem.* **2012**, *22*, 4491−4501.

(24) Frisch, M. J.; Trucks, G. W.; Schlegel, H. B.; Scuseria, G. E.; Robb, M. A.; Cheeseman, J. R.; Scalmani, G.; Barone, V.; Mennucci, B.; Petersson, G. A.; Nakatsuji, H.; Caricato, M.; Li, X.; Hratchian, H. P.; Izmaylov, A. F.; Bloino, J.; Zheng, G.; Sonnenberg, J. L.; Hada, M.; Ehara, M.; Toyota, K.; Fukuda, R.; Hasegawa, J.; Ishida, M.; Nakajima, T.; Honda, Y.; Kitao, O.; Nakai, H.; Vreven, T.; Montgomery, J. J. A.; Peralta, J. E.; Ogliaro, F.; Bearpark, M.; Heyd, J. J.; Brothers, E.; Kudin, K. N.; Staroverov, V. N.; Kobayashi, R.; Normand, J.; Raghavachari, K.; Rendell, A.; Burant, J. C.; Iyengar, S. S.; Tomasi, J.; Cossi, M.; Rega, N.; Millam, J. M.; Klene, M.; Knox, J. E.; Cross, J. B.; Bakken, V.; Adamo, C.; Jaramillo, J.; Gomperts, R.; Stratmann, R. E.; Yazyev, O.; Austin, A. J.; Cammi, R.; Pomelli, C.; Ochterski, J. W.; Martin, R. L.; Morokuma, K.; Zakrzewski, V. G.; Voth, G. A.; Salvador, P.; Dannenberg, J. J.; Dapprich, S.; Daniels, A. D.; Farkas, Ö.; Foresman, J. B.; Ortiz, J. V.; Cioslowski, J.; Fox, D. J. *Gaussian*; Gaussian Inc.: Wallingford, CT, 2009.

(25) Minaev, B.; Agren, H. *Chem. Phys.* **2005**, *315*, 215−239.

(26) Koseki, S.; Fedorov, D. G.; Schmidt, M. W.; Gordon, M. S. *J. Phys. Chem. A* **2001**, *105*, 8262−8268.

(27) Koseki, S.; Schmidt, M. W.; Gordon, M. S. *J. Phys. Chem. A* **1998**, *102*, 10430−10435.

(28) Jansson, E.; Norman, P.; Minaev, B.; Agren, H. *J. Chem. Phys.* **2006**, *124*, 114106−7.

(29) Li, X.; Minaev, B.; Ågren, H.; Tian, H. *J. Phys. Chem. C* **2011**, *115*, 20724−20731.

(30) Jansson, E.; Minaev, B.; Schrader, S.; Ågren, H. *Chem. Phys.* **2007**, *333*, 157−167.

(31) Li, X.; Zhang, Q.; Tu, Y.; Agren, H.; Tian, H. *Phys. Chem. Chem. Phys.* **2010**, *12*, 13730−13736.

(32) Matsushita, T.; Asada, T.; Koseki, S. *J. Phys. Chem. C* **2007**, *111*, 6897−6903.

(33) *Dalton*, a molecular electronic structure program; Dalton: 2011; available online: http://daltonprogram.org.

(34) Hajgato, B.; Szieberth, D.; Geerlings, P.; De Proft, F.; Deleuze, M. S. *J. Chem. Phys.* **2009**, *131*, 224321.

(35) Padhye, M. R.; McGlynn, S. P.; Kasha, M. *J. Chem. Phys.* **1956**, *24*, 588−594.

(36) Leang, S. S.; Zahariev, F.; Gordon, M. S. *J. Chem. Phys.* **2012**, *136*, 104101.

(37) Sears, J. S.; Koerzdoerfer, T.; Zhang, C.; Bredas, J. *J. Chem. Phys.* **2011**, *135*, 151103.

(38) Pedash, Y. F.; Prezhdo, O. V.; Kotelevskiy, S. I.; Prezhdo, V. V. *J. Mol. Struct.: THEOCHEM* **2002**, *585*, 49−59.

(39) Nicklass, A.; Peterson, K. A.; Berning, A.; Werner, H.; Knowles, P. J. *J. Chem. Phys.* **2000**, *112*, 5624−5632.

(40) Berning, A.; Schweizer, M.; Werner, H.; Knowles, P. J.; Palmieri, P. *Mol. Phys.* **2000**, *98*, 1823−1833.

(41) Gastilovich, E.; Klimenko, V.; Korol Kova, N.; Nurmukhametov, R.; Serov, S. *Opt. Spectrosc.* **2008**, *105*, 38−45−45.

(42) Turro, N. J. *Modern Molecular Photochemistry*; Benjamin/ Cummings Publishing Co., Inc.: San Francisco, CA, 1978; p 186.

(43) Gastilovich, E.; Klimenko, V.; Korol Kova, N.; Nurmukhametov, R.; Serov, S. *Opt. Spectrosc.* **2008**, *105*, 38−45−45.

(44) Nijegorodov, N.; Vasilenko, V.; Monowe, P.; Masale, M. *Spectrochim. Acta Part A: Mol. Biomol. Spectrosc.* **2009**, *74*, 188−194.

(45) Breu, J.; Stössel, P.; Schrader, S.; Starukhin, A.; Finkenzeller, W. J.; Yersin, H. *Chem. Mater.* **2005**, *17*, 1745−1752.

(46) Endo, A.; Suzuki, K.; Yoshihara, T.; Tobita, S.; Yahiro, M.; Adachi, C. *Chem. Phys. Lett.* **2008**, *460*, 155−157.

(47) Finkenzeller, W. J.; Yersin, H. *Chem. Phys. Lett.* **2003**, *377*, 299−305.

(48) Hofbeck, T.; Yersin, H. *Inorg. Chem.* **2010**, *49*, 9290−9299.

(49) Sajoto, T.; Djurovich, P. I.; Tamayo, A. B.; Oxgaard, J.; Goddard, W. A.; Thompson, M. E. *J. Am. Chem. Soc.* **2009**, *131*, 9813−9822.

(50) Smith, A. R. G.; Burn, P. L.; Powell, B. J. *ChemPhysChem* **2011**, *12*, 2429−2438.

(51) Wu, Y.; Bredas, J. *J. Chem. Phys.* **2008**, *129*, 214305−10.

(52) Yersin, H.; Rausch, A. F.; Czerwieniec, R.; Hofbeck, T.; Fischer, T. *Coord. Chem. Rev.* **2011**, *255*, 2622−2652.

(53) Li, X.; Minaev, B.; Ågren, H.; Tian, H. *Eur. J. Inorg. Chem.* **2011**, *2011*, 2517−2524.

(54) Gao, X.; Peng, Q.; Niu, Y.; Wang, D.; Shuai, Z. *Phys. Chem. Chem. Phys.* **2012**, *14*, 14207−14216.